

StableIntrinsic: Detail-preserving One-step Diffusion Model for Multi-view Material Estimation

XIUCHAO WU*, State Key Lab of CAD&CG, Zhejiang University, China and Alibaba Group, China

PENGFEI ZHU*, State Key Lab for Novel Software Technology, Nanjing University, China and Alibaba Group, China

JIANGJING LYU†, Alibaba Group, China

XINGUO LIU, State Key Laboratory of CAD&CG, Zhejiang University, China

JIE GUO, State Key Lab for Novel Software Technology, Nanjing University, China

YANWEN GUO, State Key Lab for Novel Software Technology, Nanjing University, China

WEIWEI XU, State Key Lab of CAD&CG, Zhejiang University, China

CHENGFEI LYU‡, Alibaba Group, China

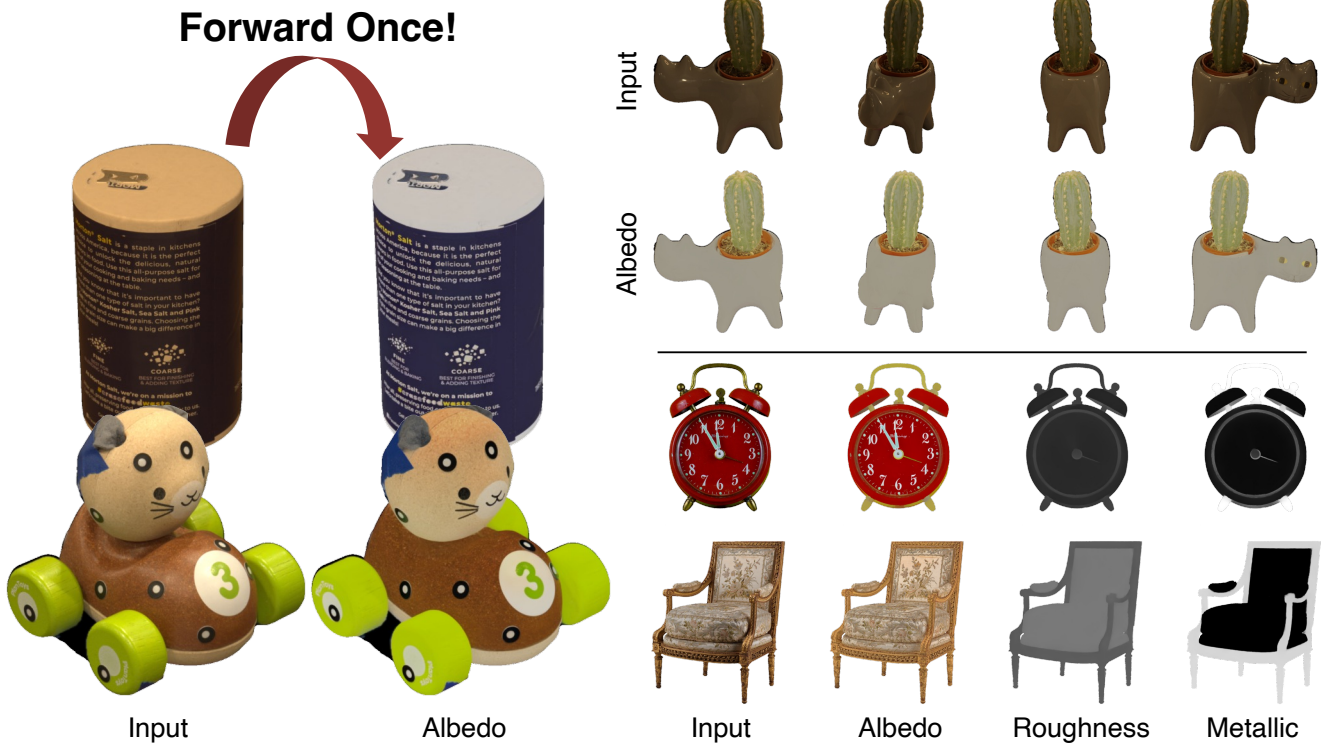


Fig. 1. **Estimated results of StableIntrinsic.** **Left:** StableIntrinsic estimates material information from RGB images in a single step, producing results with preserved details; **Top right:** StableIntrinsic supports multi-view material estimation and can output globally consistent material maps; **Bottom right:** StableIntrinsic can accurately estimate material parameters for different types of objects.

*Joint first authors

†Project leader

‡Corresponding author

Authors' addresses: Xiuchao Wu, wuxiuchao@zju.edu.cn, State Key Lab of CAD&CG, Zhejiang University, China and Alibaba Group, China; Pengfei Zhu, pfzhu@smail.nju.edu.cn, State Key Lab for Novel Software Technology, Nanjing University, China and Alibaba Group, China; Jiangjing Lyu, jiangjing.lj@taobao.com, Alibaba Group, China; Xinguo Liu, xgliu@cad.zju.edu.cn, State Key Laboratory of CAD&CG, Zhejiang University, China; Jie Guo, guojie@nju.edu.cn, State Key Lab for Novel Software Technology, Nanjing University, China; Yanwen Guo, ywguo@nju.edu.cn, State Key Lab for Novel Software Technology, Nanjing University, China; Weiwei Xu, xww@

Recovering material information from images has been extensively studied in computer graphics and vision. Recent works in material estimation leverage diffusion model showing promising results. However, these diffusion-based methods adopt a multi-step denoising strategy, which is time-consuming for each estimation. Such stochastic inference also conflicts with the deterministic material estimation task, leading to a high variance estimated results. In this paper, we introduce StableIntrinsic, a one-step diffusion model for multi-view material estimation that can produce high-quality

cad.zju.edu.cn, State Key Lab of CAD&CG, Zhejiang University, China; Chengfei Lyu, chengfei.lcf@taobao.com, Alibaba Group, China.

material parameters with low variance. To address the overly-smoothing problem in one-step diffusion, StableIntrinsic applies losses in pixel space, with each loss designed based on the properties of the material. Additionally, StableIntrinsic introduces a Detail Injection Network (DIN) to eliminate the detail loss caused by VAE encoding, while further enhancing the sharpness of material prediction results. The experimental results indicate that our method surpasses the current state-of-the-art techniques by achieving a 9.9% improvement in the Peak Signal-to-Noise Ratio (PSNR) of albedo, and by reducing the Mean Square Error (MSE) for metallic and roughness by 44.4% and 60.0%, respectively.

CCS Concepts: • **Computing methodologies** → **Image manipulation**.

Additional Key Words and Phrases: One-step Diffusion Model, Multi-view Material Estimation, Detail Preservation

1 INTRODUCTION

Intrinsic image decomposition is a long-standing challenge aiming to retrieve the surface reflectance property and the effects of illumination separately. The former, known as material estimation, is a fundamental but ill-posed problem [Grosse et al. 2009]. In light of the remarkable success of diffusion-based generative models [Ho et al. 2020; Rombach et al. 2022] in dense perception tasks, recent works [Li et al. 2024; Xi et al. 2024; Zeng et al. 2024a] integrate these models into material estimation to address the issue of overly-smoothing and detail-lacking results of regression-based methods. This is achieved through dozens to hundreds of forward passes using the UNet architecture to denoise Gaussian noise [Rombach et al. 2022; Song et al. 2020], which typically requires several to tens of seconds for inference on a general graphics card.

In addition to inefficiency, these approaches also suffer from inherent stochasticity. As shown in Fig. 2, the results generated by this kind of approach often exhibit significant variance. For albedo, as high-frequency areas are more easily affected by the input Gaussian noise, these areas have high variance across different samples, leading to various generated textures. Although these textures might seem perceptually correct, the misalignment with actual labels results in substantial pixel-level errors. For roughness and metallic, as the images are captured under uncontrollable illumination, the ambiguity in disentangling reflection causes multiple possible explanations of the material. Although the correct one usually has the highest probability of being produced, the randomness of input Gaussian noise might still affect the model to produce those low-probability incorrect explanations. This is often observed for glossy regions (Fig. 2 bottom). Such significant variance makes it unreliable and limits its applicability for deterministic tasks. Overall, it is necessary to develop an efficient and low-variance model for material estimation.

To this end, we propose StableIntrinsic, a diffusion-based model that can estimate material parameters from multi-view RGB images in a single step (Fig. 1). Instead of forwarding multiple times for denoising, StableIntrinsic only needs to forward once, resulting in a significant acceleration of the estimation process. It also naturally lowers the variance of the output results (Fig. 2). The key challenge of one-step diffusion model is the blurry output. To overcome this, rather than optimizing in feature space, which is ineffective for producing higher quality results (Fig. 3), we choose to optimize StableIntrinsic in pixel space [Xu et al. 2024]. This effectively improves

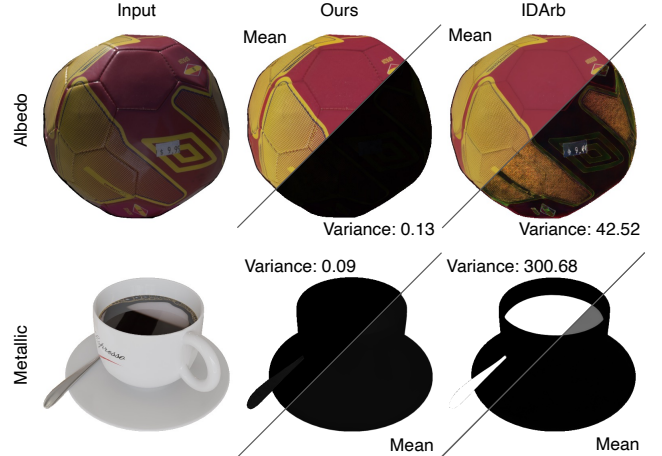


Fig. 2. **Low-variance material estimation of StableIntrinsic.** We use multiple different random noise to inference and visualize the mean and variance of the predicted material maps for StableIntrinsic and SOTA method IDArb [Li et al. 2024].



Fig. 3. **Overly-smoothing problem of applying loss in feature space.**

the output results, especially in high-frequency areas. Additionally, images with rich detailed textures fail to be well preserved in estimated results as the VAE breaks the structure information of them after encoding. We thus introduce a Detail Injection Network (DIN) to further correct the results and enhance the sharpness. In general, StableIntrinsic has three contributions:

- To the best of our knowledge, StableIntrinsic is the first one-step diffusion model for material estimation, which significantly accelerates inference and enhances estimation stability.
- We address the overly-smoothing problem of one-step denoising by optimizing StableIntrinsic in pixel space and introducing a Detail Injection Network (DIN).
- Extensive experiments show that StableIntrinsic outperforms state-of-the-art methods, showing high quality estimated albedo with rich details, and accurate metallic and roughness.

2 RELATED WORKS

2.1 Learning-based Material Estimation

The material estimation task aims to disentangle the surface material properties and environment illumination from images [Barron and Malik 2013, 2015; Chen and Koltun 2013; Garces et al. 2012; Grosse et al. 2009], which is discussed in detail in Garces et al. [2022]. Recent

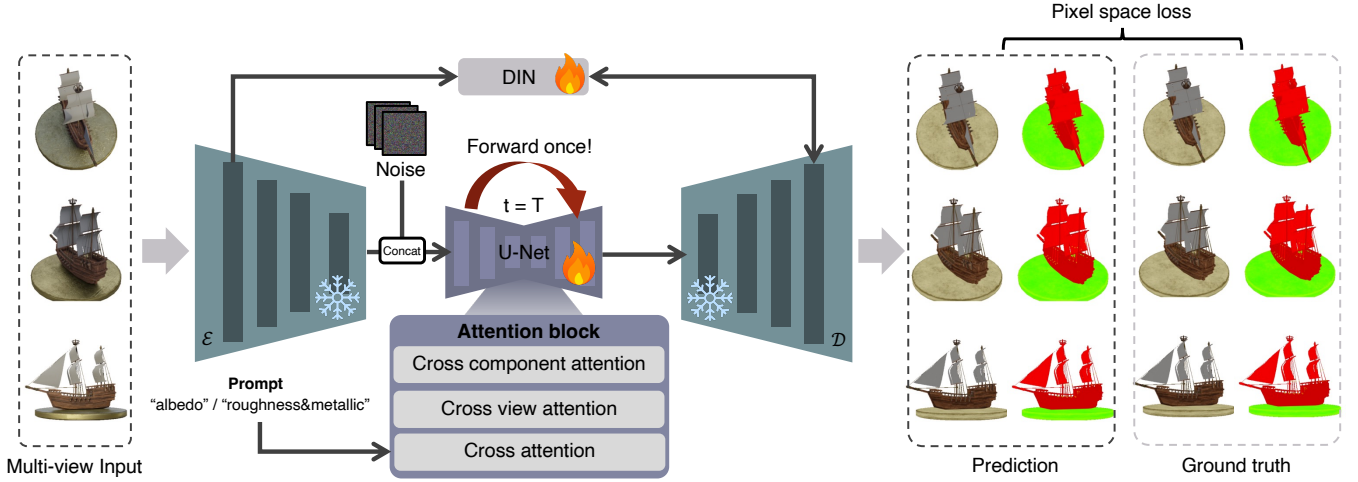


Fig. 4. **An overview of our method.** StableIntrinsic predicts material parameters of multi-view RGB images in one-step. We optimize our model in pixel space to enhance the acquisition of fine-grained details. Based on the property of each material, we use different loss for albedo A and roughness&metallic RM . To compensate for the quality degradation caused by VAE encoding, we introduce a Detail Injection Network (DIN) to further improve the output results.

advancements in deep learning have led to significant improvements in this field [Azinovic et al. 2019; Li et al. 2020; Philip et al. 2021; Wang et al. 2021; Zhu et al. 2022], surpassing previous methods. They use feed-forward models to decompose images, but due to the ambiguities of material and illumination, they often produce blurry results lacking high-frequency details [Kocsis et al. 2024].

Generative models have attracted widespread attention and discussion in multiple fields [Rombach et al. 2022]. Leveraging prior learning from a massive number of high-fidelity images, diffusion-based models have demonstrated strong capabilities across various vision tasks [Fu et al. 2024; He et al. 2025a; Ke et al. 2024; Liang et al. 2025; Xu et al. 2024; Ye et al. 2024; Zeng et al. 2024b]. Several studies have used these models as pre-trained foundations, fine-tuning them for intrinsic decomposition [He et al. 2025b; Huang et al. 2024; Kocsis et al. 2024; Li et al. 2024; Luo et al. 2024; Xi et al. 2024; Zeng et al. 2024a; Zhang et al. 2024]. Although the results that are more consistent with visual perception are achieved compared to regression-based approaches, these models have limitations. Single-image methods suffer from multiview inconsistency [Kocsis et al. 2024; Xi et al. 2024; Zeng et al. 2024a]. IDArb [Li et al. 2024] enhances multiview consistency with additional attention blocks but struggles with incorrect texture structures disrupted by the outermost auto-encoder and tends to oversimplify complex real-world objects. Moreover, these models often require dozens to hundreds of forward passes of the neural network, resulting in slow and costly inference, limiting their applicability to downstream tasks.

2.2 One-step Diffusion-based Estimation

Trivially rescheduling the noises into fewer steps or a single-step denoising often results in low-quality generation [Song et al. 2020]. Therefore, accelerating the sampling process has been a topic of extensive discussion, exploring methods such as distillation models [Meng et al. 2022; Salimans and Ho 2022; Yin et al. 2024], Rectified

Flow [Liu et al. 2022, 2024], Consistency Models [Song et al. 2023], and Shortcut Models [Frans et al. 2025].

When utilizing diffusion-based models in vision tasks, the strong correspondence between conditional images and ground-truth labels facilitates reconstruction, yielding clean results in single-step denoising scenarios. Various studies [He et al. 2025a; Martin Garcia et al. 2025; Xu et al. 2024; Ye et al. 2024] have shown that single-step forward delivers comparable results in dense perception tasks. Recognizing the instability due to stochastic nature of diffusion models, these studies propose deterministic approaches that exclude noisy inputs. Nevertheless, they still struggle to recover high-frequency details. To overcome this issue, GenPercept [Xu et al. 2024] further substitutes the original decoder with a task-specific one and employs pixel-wise losses to enhance results. Lotus [He et al. 2025a] applies a reconstruction task as regularization, whereas StableNormal [Ye et al. 2024] utilizes a two-stage denoising framework with semantic-guided refinement.

Material estimation, a special case of dense perception tasks, necessitates detail preservation, highlight-shadow removal, and recovery of semantic-consistent material parameters. Building on prior works, our method adjusts sampling and regularization strategies to address this complex task, achieving superior performance.

3 METHOD

StableIntrinsic is a diffusion-based model, which aims to estimate high-quality PRB material (i.e. albedo A , roughness R and metallicity M) parameters from multi-view RGB images efficiently. To this end, we make the denoising process a single step to accelerate the estimation process, which also reduces the variance in the predicted material maps (Fig. 2). To address the overly-smoothing problem of one-step estimation, we choose to optimize StableIntrinsic with pixel space losses (Sec. 3.2). Finally, we introduce a detail-injection

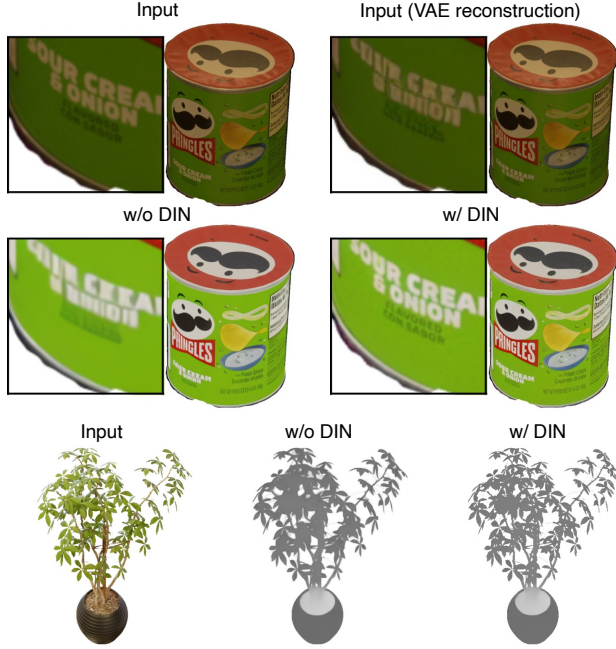


Fig. 5. **DIN effectively injects details.** **Top:** VAE fails to reconstruct input condition images with rich details; **Mid:** DIN can successfully inject details to predicted albedo map while avoiding introducing reflections from the lid of this can; **Bottom:** DIN enhances the sharpness of predicted roughness.

module to further improve the output results (Sec. 3.3). An overview of our method is shown in Fig. 4.

3.1 Preliminary

Given a random noise $\mathbf{z}_T \sim \mathcal{N}(\mathbf{0}, \mathbf{I})$, the latent diffusion model [Rom-bach et al. 2022] sequentially denoises it into a target data \mathbf{z}_0 by predicting noise ϵ_t at each time step t . The noise is typically output by a neural network μ_θ , which can be optimized with loss for v-parameterization [Salimans and Ho 2022]:

$$L_\theta = \mathbb{E}_{\epsilon \sim \mathcal{N}(\mathbf{0}, \mathbf{I}), \mathbf{z}_c, t} \|\mathbf{v} - \mu_\theta(\mathbf{z}_t, t, \mathbf{z}_c)\|_2^2, \quad (1)$$

$$\mathbf{v} = \sqrt{\bar{\alpha}_t} \epsilon - \sqrt{1 - \bar{\alpha}_t} \mathbf{z}_0, \quad (2)$$

where $\mathbf{z}_c = \mathcal{E}(\mathbf{I})$ is the latent feature of a condition image \mathbf{I} encoded by a pre-trained VAE [Kingma et al. 2013] encoder \mathcal{E} . $\bar{\alpha}_t$ is the noise schedule that controls the proportion of noise. \mathbf{z}_t is sampled by adding noise to \mathbf{z}_0 :

$$\mathbf{z}_t = \sqrt{\bar{\alpha}_t} \mathbf{z}_0 + \sqrt{1 - \bar{\alpha}_t} \epsilon, \epsilon \sim \mathcal{N}(\mathbf{0}, \mathbf{I}), t \in \{0, 1, \dots, T\}. \quad (3)$$

The one-step denoising aims to predict \mathbf{z}_0 from \mathbf{z}_T directly, which is a pure Gaussian noise ($\mathbf{z}_T = \epsilon$) as $\bar{\alpha}_T = 0$. Therefore, Equ. 1 can be reformulated as:

$$L_\theta = \mathbb{E}_{\epsilon \sim \mathcal{N}(\mathbf{0}, \mathbf{I}), \mathbf{z}_c, t=T} \|\mathbf{z}_0 - \mu_\theta(\epsilon, T, \mathbf{z}_c)\|_2^2. \quad (4)$$

In this case, the output of μ_θ is constrained to predict the negative \mathbf{z}_0 (Equ. 2). As a result, instead of optimizing across different time steps, one-step denoising only needs to be optimized at time step T .

3.2 One-step material estimation

Unfortunately, simply denoising in a single step with a diffusion model is almost unable to produce details, showing overly-smoothing prediction results. To address this problem, we optimize our model in pixel space, which is similar to GenPercept [Xu et al. 2024] and generally has two benefits:

- (1) Since the resolution of output images is 8 times than that of latent features, our loss is calculated at a higher resolution, which can help μ_θ produce results with more details (Fig. 3);
- (2) Based on the properties of albedo, roughness and metallicity, we can choose different types of losses for them to achieve higher-quality results (Fig. 9).

Therefore, the optimization of our one-step material estimation model can be formulated as:

$$L_\theta = \mathbb{E}_{\epsilon \sim \mathcal{N}(\mathbf{0}, \mathbf{I}), \mathbf{z}_c, t=T} \|\mathbf{K} - \mathcal{D}(\mu_\theta(\epsilon \mathbf{z}_c, T))\|_2^2, \quad (5)$$

where \mathcal{D} is a pre-trained VAE [Kingma et al. 2013] decoder corresponding to the encoder \mathcal{E} . $\mathbf{K} \in \{\mathbf{A}, \mathbf{RM}\}$ is the target material, including albedo $\mathbf{A} \in \mathbb{R}^{H \times W \times 3}$ and roughness&metallic $\mathbf{RM} \in \mathbb{R}^{H \times W \times 3}$, where $\mathbf{RM} = [\mathbf{R}^{H \times W \times 1}, \mathbf{M}^{H \times W \times 1}, \mathbf{O}^{H \times W \times 1}]$. The input condition \mathbf{z}_c is concatenated with ϵ before feeding to μ_θ .

During training, we use an MSE loss to supervise albedo $\hat{\mathbf{A}}$ and roughness and metallic $\hat{\mathbf{RM}}$. In addition, we use a gradient matching loss [Li and Snavely 2018] for $\hat{\mathbf{RM}}$ to improve the sharpness of their boundaries:

$$L_{GM}(\mathbf{RM}, \hat{\mathbf{RM}}) = \frac{1}{N} (\|\nabla_x(\hat{\mathbf{RM}} - \mathbf{RM})\|_1^1 + \|\nabla_y(\hat{\mathbf{RM}} - \mathbf{RM})\|_1^1), \quad (6)$$

where N is the total number of pixels, and ∇_x/∇_y denotes the gradient in x/y direction. Compared to the MSE loss, which calculates the loss for each pixel equally, L_{GM} is calculated based on neighboring pixels and focuses on penalizing areas with unmatched gradients (e.g., blurred \mathbf{RM} boundaries or incorrectly baked textures), thereby helping preventing texture baking in $\hat{\mathbf{RM}}$ (Fig. 9). The final loss is the combination of all above losses:

$$L_\theta = L_{\text{MSE}}(\mathbf{A}, \hat{\mathbf{A}}) + L_{\text{MSE}}(\mathbf{RM}, \hat{\mathbf{RM}}) + L_{GM}(\mathbf{RM}, \hat{\mathbf{RM}}). \quad (7)$$

3.3 Detail Refinement

Although optimizing in pixel space can enhance the sharpness of output results, achieving a comparable quality of multi-step denoising in a single step is still challenging. Furthermore, the structure information of high-frequency textures is misaligned after passing through the VAE encoder, leading to failures in detail recovery. This has a significant impact on albedo prediction, and also affects the prediction of roughness and metallic properties for objects with high-frequency geometric contours (Fig. 5).

Inspired by [Xu et al. 2025; Zhu et al. 2023], we introduce a detail injection network (DIN) f_ϕ , which can effectively improve the prediction details by modulating the hidden features of \mathcal{D} :

$$H_{\mathcal{D}} = f_\phi(\text{concat}(H_{\mathcal{E}}, H_{\mathcal{D}})) + H_{\mathcal{D}}, \quad (8)$$

where $H_{\mathcal{E}}$ and $H_{\mathcal{D}}$ are hidden features of encoder \mathcal{E} and decoder \mathcal{D} respectively, and are concatenated along the channel dimension. Both $H_{\mathcal{E}}$ and $H_{\mathcal{D}}$ are high resolution features, which typically have more detailed information and are suitable for detail injection. As

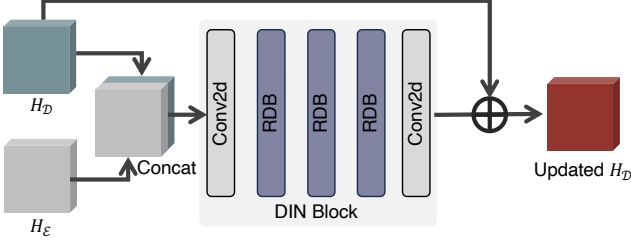


Fig. 6. The architecture of Detail Injection Network (DIN).

shown in Fig. 6, DIN consists of a set of Residual Dense Blocks (RDB) [Zhang et al. 2018], which is originally designed for image super-resolution. It takes the concatenation of H_E and H_D as input and outputs a new feature to update H_D .

Although DIN doesn’t incorporate cross-view attention to ensure consistency, we didn’t observe inconsistency issues in most cases (Fig. 15 presents two examples in the multi-view setting). We believe this is because the injected high-frequency structures are naturally multi-view consistent in the original RGB images (e.g., text details are generally consistent across views). Even when there are inconsistent features, such as highlights, reflections, and varying illumination, DIN can still effectively avoid introducing these features. This benefits from being trained on such data and leveraging the denoised multi-view consistent material features H_D as a reference.

3.4 Discussion of low-variance

In our one-step diffusion model, the randomness of inference mainly comes from the initial Gaussian noise. As shown in Fig. 2, compared with multi-step methods, the variance of our model is sufficiently small, making it difficult to visually discern differences in estimated results across different seeds. We think this is because our model is optimized at time step T , where the input noise is a pure Gaussian noise providing limited information for material estimation. Therefore, our model shows a low sensitivity to input noise. Consequently, even if we remove the Gaussian noise input, it does not adversely affect the model’s performance.

4 IMPLEMENTATION DETAILS

Network architecture. Similar to IDArb [Li et al. 2024], we adopt cross-component and cross-view attention to improve prediction quality and enforce global consistency across different views. To switch the task between predicting A and RM , we use specific text prompts as conditions. For DIN, we directly use the RDB block from Zhang et al. [2018] and set the kernel size to 3 for all other convolutional layers. To modulate hidden features through DIN, we use the first two layers of VAE encoder \mathcal{E} to update the last two layers of VAE decoder \mathcal{D} .

Optimization. For better initializing our one-step diffusion model, we first train a multi-step diffusion model for material estimation using v-parameterization, with the same training setup as IDArb [Li et al. 2024]. Then, we initialize StableIntrinsic with this pre-trained

Table 1. **Quantitative comparisons on synthetic data.** The best results are highlighted as **1st** and **2nd**. For real-world datasets, the metrics are calculated by their pseudo ground-truth maps.

Methods	Albedo		Metallic	Roughness
	SSIM \uparrow	PSNR \uparrow	MSE \downarrow	MSE \downarrow
Objaverse-Testing				
RGB \leftrightarrow X	0.861	25.42	0.068	0.035
IntrinsicAnything	0.880	26.54	-	-
IDArb	<u>0.915</u>	<u>29.73</u>	<u>0.029</u>	<u>0.020</u>
Ours	0.949	32.67	0.015	0.008
ShinyBlender [Verbin et al. 2022]				
RGB \leftrightarrow X	0.861	22.54	0.101	0.144
IntrinsicAnything	0.893	26.34	-	-
IDArb	<u>0.951</u>	<u>30.20</u>	<u>0.009</u>	<u>0.004</u>
Ours	0.973	34.28	0.005	0.002

Table 2. **Quantitative comparisons on real-world data.** We compare our **albedo** results against other baselines. The best results are highlighted as **1st**, **2nd**. The metrics are calculated using the pseudo ground-truth maps.

Methods	Stanford-ORB		MIT-Intrinsic	
	SSIM \uparrow	PSNR \uparrow	SSIM \uparrow	PSNR \uparrow
RGB \leftrightarrow X	0.839	30.23	0.793	22.43
IntrinsicAnything	0.847	31.83	<u>0.822</u>	<u>24.42</u>
IDArb	<u>0.866</u>	32.57	0.811	22.84
Ours	0.882	<u>32.33</u>	0.842	25.72

model and optimize μ_θ on time step T only. However, simultaneously optimizing μ_θ and f_ϕ is difficult due to the limited GPU memory. Therefore, we first use Equ. 7 to optimize μ_θ with a fixed VAE [Kingma et al. 2013]. Subsequently, we freeze all other network parameters and only optimize f_ϕ to enhance details.

Hyper-parameters configuration. For the training of U-net μ_θ and DIN f_ϕ , we use AdamW [Loshchilov and Hutter 2019] optimizer with a learning rate of 1×10^{-4} that linearly decays to 1×10^{-5} . μ_θ is trained over 10K steps with a batch size of 8 and f_ϕ is trained over 20K steps with a batch size of 4. Both μ_θ and f_ϕ are optimized using 32 AMD MI308X GPU cards.

5 EXPERIMENTS

5.1 Setup

Dataset. For training, we use the same training set as IDArb [Li et al. 2024], which employs Arb-Objaverse [Li et al. 2024], G-Objaverse [Zuo et al. 2024], and ABO [Collins et al. 2022] with a resolution of 256×256 . For evaluation, since the testing split of IDArb is unpublished, we exclude object indices present in the training set and select the remaining objects from Arb-Objaverse along with a random subset from G-Objaverse, forming the Objaverse-Testing dataset of 200 objects. To demonstrate the generalizability of our method, we also evaluate on ShinyBlender [Verbin et al. 2022] and

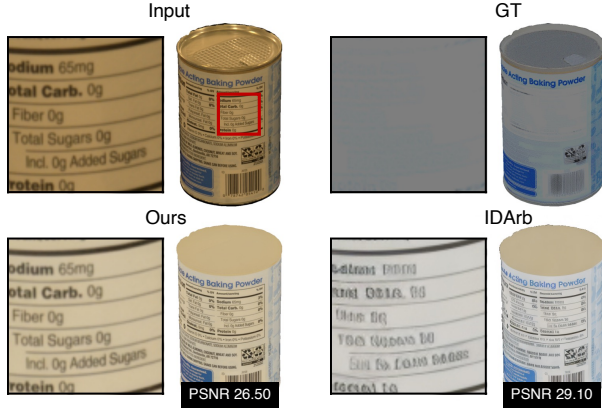


Fig. 7. **Pseudo ground-truth albedo maps of Stanford-ORB** [Kuang et al. 2023]. Since the ground truth of the Stanford-ORB dataset is pseudo, our method might achieve a lower PSNR compared to other methods, even though it produces sharper albedo maps.

Table 3. **Ablation Studies.** w/o Opt. represents that we directly use the pre-trained v-parameterization diffusion model to conduct one-step denoising. In order to eliminate the influence of DIN, the following ablations are conducted **without using DIN**, except for the last row (Ours), which is used to show the effect of DIN.

	Albedo		Metallic	Roughness
	SSIM \uparrow	PSNR \uparrow	MSE \downarrow	MSE \downarrow
w/o Opt.	0.919	30.40	0.019	0.011
w/o L_{GM}	0.929	30.83	0.018	0.011
Ours (w/o DIN)	0.932	31.33	0.016	0.009
Ours (w/ DIN)	0.949	32.67	0.015	0.008

two public real-world datasets: MIT-Intrinsic [Grosse et al. 2009] and Stanford-ORB [Kuang et al. 2023]. We sample 4 viewpoints for each object from multi-view datasets with a resolution of 512×512 for evaluation. As the background occupies a large portion that can affect quantitative comparisons, we crop each input image based on its mask to enhance the precision of metric calculations.

Baselines. To evaluate our method, we conduct comparisons with the state-of-the-art diffusion-based material estimation methods: RGB \leftrightarrow X [Zeng et al. 2024a], IntrinsicAnything [Xi et al. 2024], and IDArb [Li et al. 2024]. We utilize their pre-released models for evaluation. As IntrinsicAnything only releases the single-image inference code and does not decompose the metallicity and roughness, we adopt it for albedo comparison in the single-view setting. Note that RGB \leftrightarrow X is trained on scene data, yet it demonstrates generalizability when applied to object-centric data. Therefore, we include it as a baseline in our comparisons.

Metrics. Similar to IDArb [Li et al. 2024], we use a scale-invariant Peak Signal-to-Noise Ratio (PSNR) and Structural Similarity Index Measure (SSIM) [Wang et al. 2004] for evaluating albedo, and Mean Square Error (MSE) for evaluating metallicity and roughness.

Table 4. **Inference efficiency.** We show the time cost (in seconds) of each component during inference. The best results are highlighted as **1st**.

	Single-view			Multi-view		
	Our	IDArb	RGB \leftrightarrow X	Our	IDArb	RGB \leftrightarrow X
Encode	0.046	0.046	0.032	0.190	0.165	0.106
Denoise	0.094	5.781	3.307	0.402	26.019	10.665
Decode	0.441	0.303	0.231	1.752	1.155	0.899
Total	0.581	6.130	3.570	2.344	27.339	11.670

5.2 Comparison

A quantitative comparison on synthetic data is presented in Tab. 1, where our method achieves superior results across all datasets. For Objaverse-Testing, our model produces the best results, demonstrating its capability to effectively handle various types of objects. Two examples are shown in Fig. 12, where our model recovers the specific patterns and distinguishes reflections. For ShinyBlender, we re-rendered the images and ground-truth material maps from the original project files. Despite the minimal difference in MSE metrics between our model and IDArb, our results successfully recover metallic properties without baked reflections, as displayed in Fig. 13 in the second column. This improvement will greatly benefit downstream operations, such as inverse rendering.

For real-world data, we calculate the metrics on albedo using the pseudo ground-truth maps, as shown in Tab. 2. Our method performs slightly worse in PSNR compared to IDArb on the Stanford-ORB dataset. However, it is noteworthy that the pseudo albedo maps provided by Stanford-ORB often lack details (as exemplified in Fig. 7). Furthermore, as the images are captured under environmental illumination with varying colors, decomposing color from albedo becomes highly ambiguous. Our results demonstrate a more consistent illumination decomposition across the entire object, although this does not translate into higher metric scores. We display more qualitative results in Fig. 11 and 13. While other approaches struggle with the loss of structured details and the stochastic generation of high-frequency textures, our model recovers the fine-grained textures and more plausible material properties.

Tab. 4 shows the inference efficiency comparison for both single-view and multi-view settings, tested on a single NVIDIA Tesla V100 GPU card. Since both IDArb and RGB \leftrightarrow X require 50 denoising steps (default setting), our method achieves a denoising speed approximately 50 times faster than IDArb and 30 times faster than RGB \leftrightarrow X (Note that RGB \leftrightarrow X does not incorporate cross-view/cross-component attention, making its denoising slightly faster than IDArb, but it lacks multi-view consistency.). Additionally, the introduction of DIN results in our decoding being slightly slower than that of the other methods. Overall, our model is significantly more efficient than the others.

5.3 Ablation Studies

Detail Inject Network. We disable the DIN to evaluate its impact. For albedo, as shown in Fig. 5, DIN can effectively improve the details and correct the structure information, making the letters on the can as clear as the input condition image. For roughness and metallic,



Fig. 8. **StableIntrinsic improves the results of one-step diffusion model.** **Top:** estimated albedo maps; **Bottom:** estimated roughness maps.

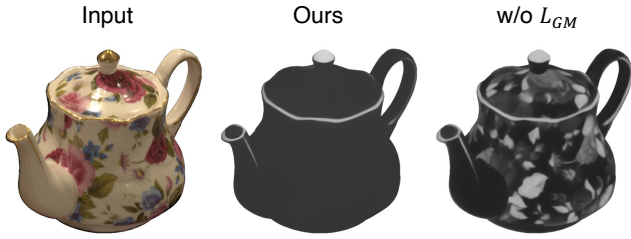


Fig. 9. **Ablation of loss L_{GM} .** Applying L_{GM} makes the predicted metallic of teapot more accurate.

DIN improves them by enhancing the sharpness of boundaries (Fig. 5 bottom). Since albedo contains more texture information, the improvement effect of DIN on albedo is more significant compared to roughness and metallic (Tab. 3).

Optimization. To demonstrate the necessity of further optimization on $t = T$, we compare our results with one-step denoising results of the pre-trained diffusion model (Tab. 3). We set the number of DDIM steps to 1 ($t = T$) for the pre-trained model to obtain the one-step denoising results. Fig. 8 shows that, without optimization, one-step denoising produces blurry and incorrect results, while our model estimates sharper albedo and more accurate roughness.

Gradient matching loss. The gradient matching loss L_{GM} prevents textures from being baked into the predicted roughness and metallic maps (Fig. 9). Although L_{GM} is only applied to roughness and metallic, removing L_{GM} leads to decreased PSNR and SSIM scores of the predicted albedo as well (Tab. 3). This might be because a lower quality of roughness or metallic influences the estimation of albedo through cross-component attention.

More results. We conduct extra experiments to fully show the capability of the model. Fig. 14 presents more results on real data collected from the Internet¹, and Fig. 15 demonstrates the consistency across multiple views.

¹<https://pixabay.com/>

Furthermore, the predicted results can be applied to enhance the material decomposition for inverse rendering. Specifically, we leverage the predictions of our model to supervise NVDiffRec [Munkberg et al. 2022] during the optimization of albedo and RM maps by applying an MSE loss. As shown in Fig. 16, the inverse rendering framework, guided by our priors, achieves a more plausible decomposition of materials and illumination, demonstrating the practical value of StableIntrinsic for downstream applications.

6 CONCLUSION

We have demonstrated a one-step diffusion model, StableIntrinsic, which estimates material parameters from multi-view RGB images while highly preserving details. However, the estimated results of our model might be affected by the illumination conditions, showing different output results for same objects under different illuminations. While this issue does not occur within a single inference batch, it restricts the application to reconstructing material maps from a plethora of images that require to be processed in multiple batches. The source of this problem mainly comes from the limited diversity of illumination in the training dataset. In the future, the model’s capability can be enhanced by expanding the training data and increasing the diversity of lighting conditions. In addition, although our DIN can effectively inject details into the predicted results, it might incorrectly introduce some high-frequency highlights into the albedo maps. This usually occurs on objects with strong lighting and rich textures, primarily because the network struggles to distinguish between small sharp highlights and texture details (see Fig. 10 for an example). Therefore, it is highly valuable to develop a DIN with stronger capabilities in highlight awareness.

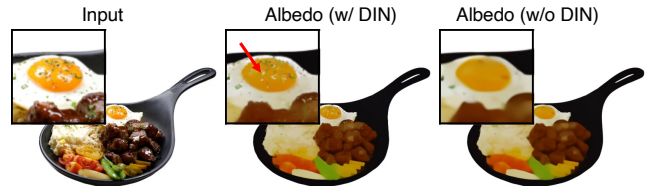


Fig. 10. **Failure case.** DIN incorrectly injects highlights in areas with details.

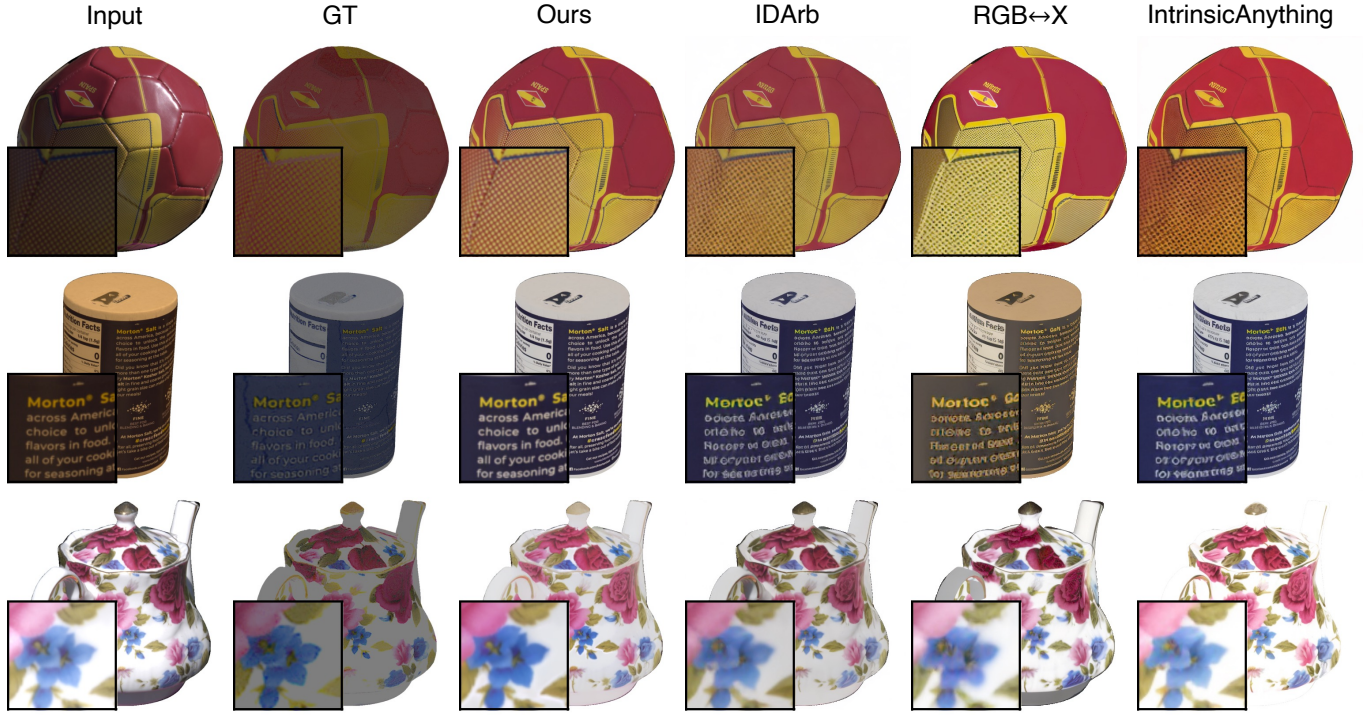


Fig. 11. Albedo qualitative comparison on public real-world data Stanford-ORB [Kuang et al. 2023]. Note that the GT maps are pseudo ground-truth albedo maps obtained from the original works, and are displayed as a reference. Our method recovers fine-grained structured textures and effectively removes highlights and shadows.

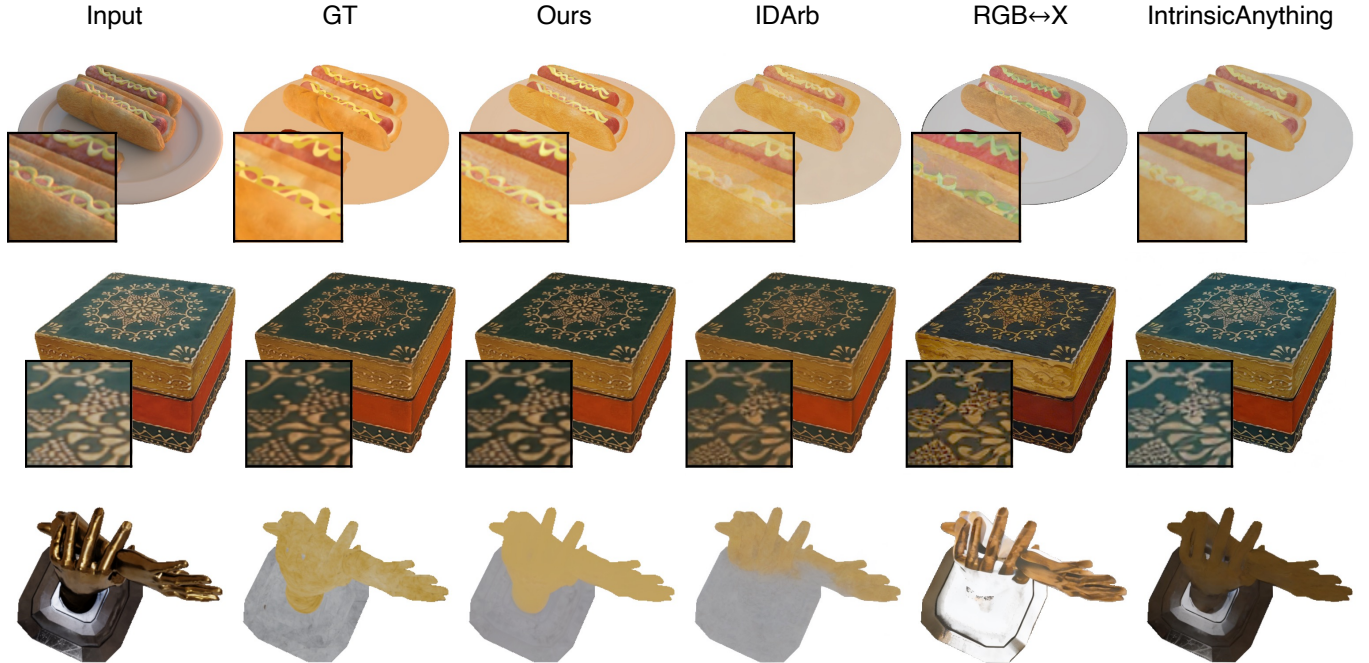


Fig. 12. Albedo qualitative comparison on synthetic data TensorIR [Jin et al. 2023] (top) and Objaverse-Testing (middle and bottom). Our method successfully preserves accurate textures and reliably distinguishes reflections, resulting in the best albedo estimation.

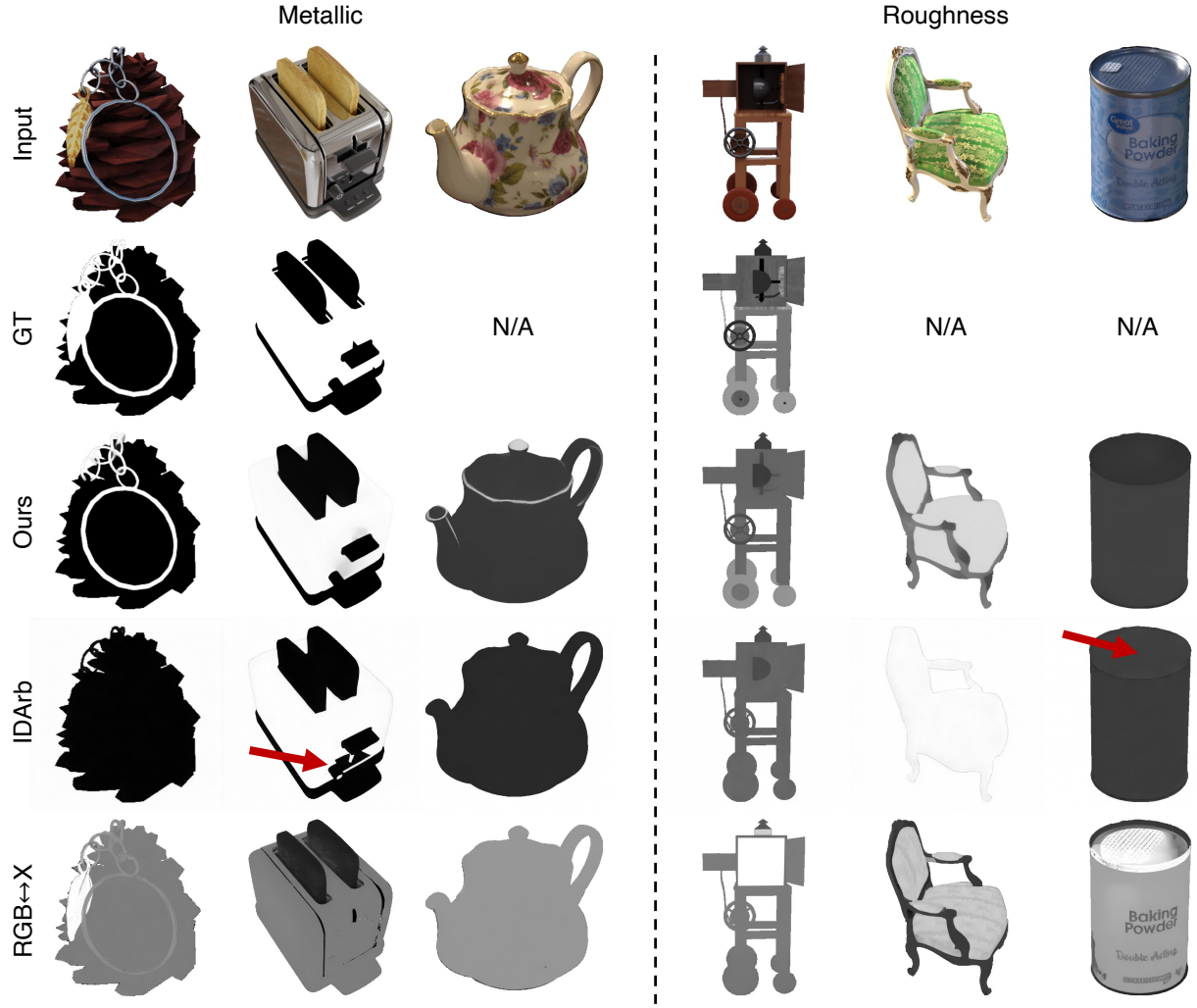


Fig. 13. **Metallicity and roughness comparison on both synthetic data and real-world data.** We use *N/A* to indicate that no ground-truth is available for this data. While IDArb [Li et al. 2024] has the limitation of oversimplification, our method stably eliminates the influence of shadows and reflections, and produces more plausible results for parts with varying material properties.

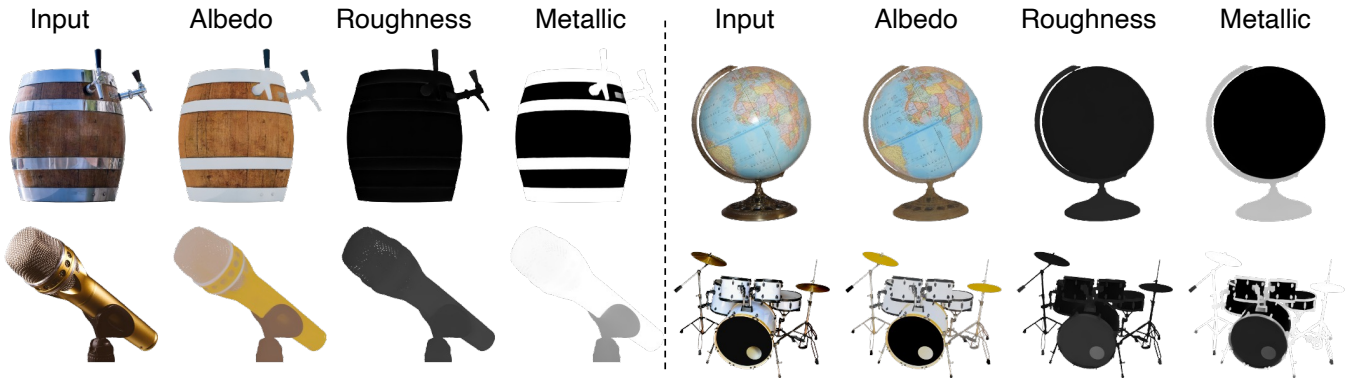


Fig. 14. **Results on real data.**

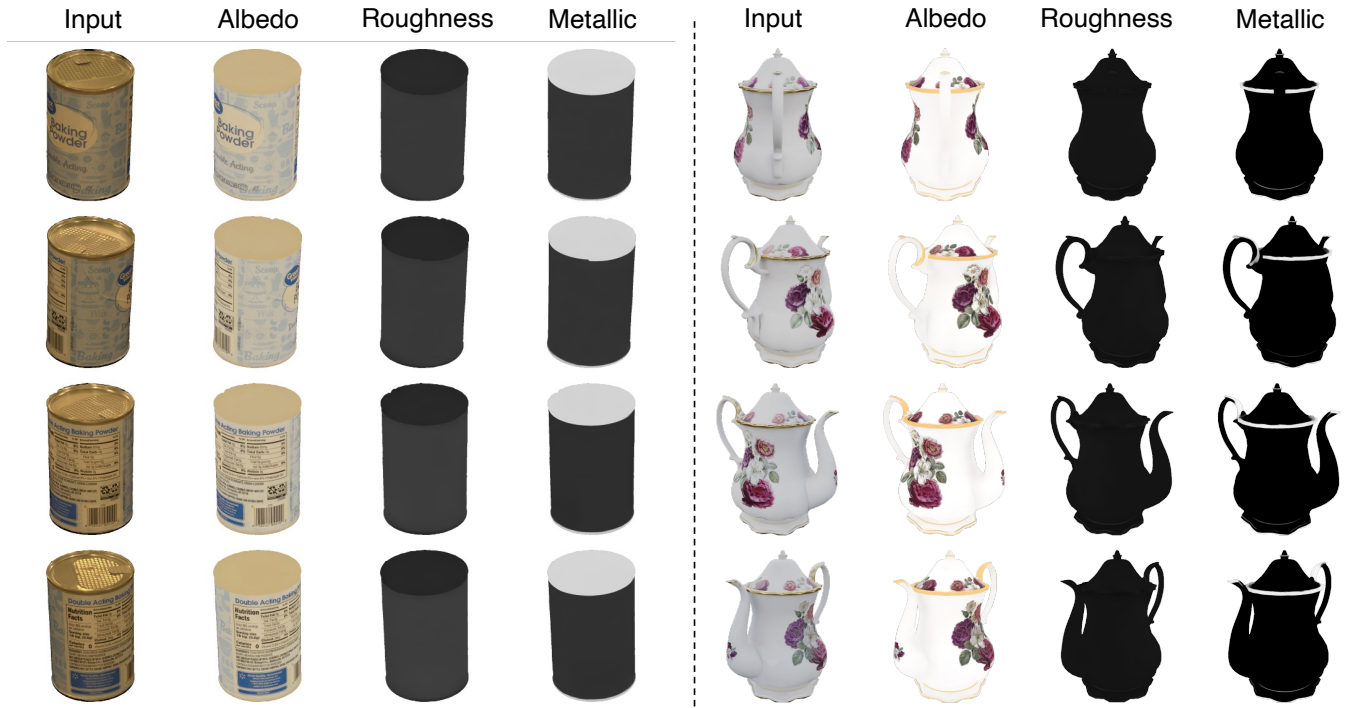
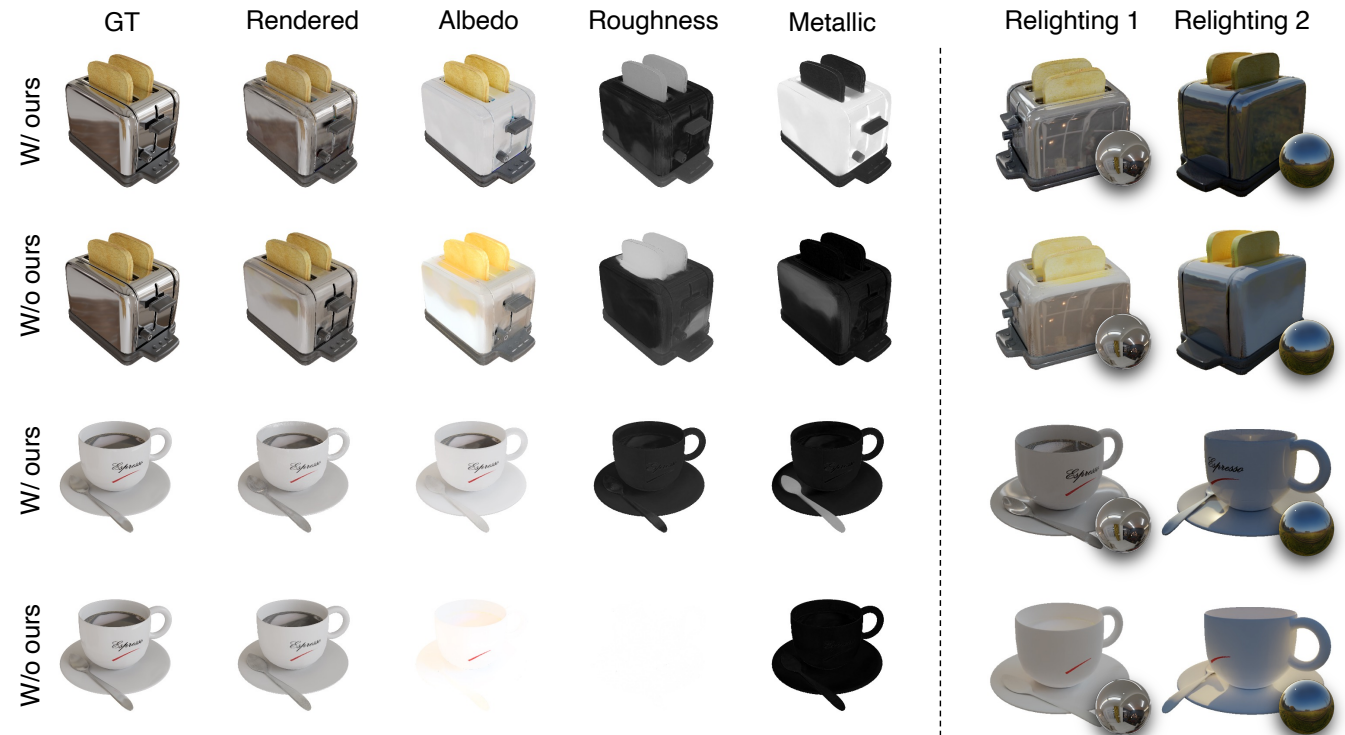


Fig. 15. Multi-view estimated results.

Fig. 16. **Applications.** We show the reconstructed results of NVDiffRec [Munkberg et al. 2022] both with and without supervision from our model’s predictions.

REFERENCES

- Dejan Azinovic, Tzu-Mao Li, Anton Kaplanyan, and Matthias Niessner. 2019. Inverse Path Tracing for Joint Material and Lighting Estimation. In *IEEE Conf. Comput. Vis. Pattern Recog.*
- Jonathan T. Barron and Jitendra Malik. 2013. Intrinsic Scene Properties from a Single RGB-D Image. In *Int. Conf. Comput. Vis.* 17–24. <https://doi.org/10.1109/CVPR.2013.10>
- Jonathan T. Barron and Jitendra Malik. 2015. Shape, Illumination, and Reflectance from Shading. *IEEE Trans. Pattern Anal. Mach. Intell.* (2015).
- Qifeng Chen and Vladlen Koltun. 2013. A Simple Model for Intrinsic Image Decomposition with Depth Cues. In *Int. Conf. Comput. Vis.* 241–248. <https://doi.org/10.1109/ICCV.2013.37>
- Jasmine Collins, Shubham Goel, Kenan Deng, Achleshwar Luthra, Leon Xu, Erhan Gundogdu, Xi Zhang, Tomas F Yago Vicente, Thomas Dideriksen, Himanshu Arora, Matthieu Guillaumin, and Jitendra Malik. 2022. ABO: Dataset and Benchmarks for Real-World 3D Object Understanding. In *CVPR*.
- Kevin Frans, Daniyar Hafner, Sergey Levine, and Pieter Abbeel. 2025. One Step Diffusion via Shortcut Models. In *Int. Conf. Learn. Represent.*
- Xiao Fu, Wei Yin, Mu Hu, Kaixuan Wang, Yuexin Ma, Ping Tan, Shaojie Shen, Dahua Lin, and Xiaoxiao Long. 2024. GeoWizard: Unleashing the Diffusion Priors for 3D Geometry Estimation from a Single Image. In *Eur. Conf. Comput. Vis.*
- Elena Garces, Adolfo Munoz, Jorge Lopez-Moreno, and Diego Gutierrez. 2012. Intrinsic Images by Clustering. *Comput. Graph. Forum* 31, 4 (2012), 1415–1424.
- Elena Garces, Carlos Rodriguez-Pardo, Dan Casas, and Jorge Lopez-Moreno. 2022. A Survey on Intrinsic Images: Delving Deep into Lambert and Beyond. *Int. J. Comput. Vis.* 130, 3 (March 2022), 836–868. <https://doi.org/10.1007/s11263-021-01563-8>
- Roger Grosse, Micah K. Johnson, Edward H. Adelson, and William T. Freeman. 2009. Ground truth dataset and baseline evaluations for intrinsic image algorithms. In *Int. Conf. Comput. Vis.* 2335–2342. <https://doi.org/10.1109/ICCV.2009.5459428>
- Jing He, Haodong Li, Wei Yin, Yixun Liang, Leheng Li, Kaiqiang Zhou, Hongbo Zhang, Bingbing Liu, and Ying-Cong Chen. 2025a. Lotus: Diffusion-based visual foundation model for high-quality dense prediction. In *Int. Conf. Learn. Represent.*
- Zexin He, Tengfei Wang, Xin Huang, Xingang Pan, and Ziwei Liu. 2025b. Neural LightRig: Unlocking Accurate Object Normal and Material Estimation with Multi-Light Diffusion. In *Proceedings of the Computer Vision and Pattern Recognition Conference*. 26514–26524.
- Jonathan Ho, Ajay Jain, and Pieter Abbeel. 2020. Denoising diffusion probabilistic models. *Adv. Neural Inform. Process. Syst.* 33 (2020), 6840–6851.
- Xin Huang, Tengfei Wang, Ziwei Liu, and Qing Wang. 2024. Material Anything: Generating Materials for Any 3D Object via Diffusion. In *IEEE Conf. Comput. Vis. Pattern Recog.*
- Haian Jin, Isabella Liu, Peijia Xu, Xiaoshuai Zhang, Songfang Han, Sai Bi, Xiaowei Zhou, Zexiang Xu, and Hao Su. 2023. TensolR: Tensorial Inverse Rendering. In *IEEE Conf. Comput. Vis. Pattern Recog.*
- Bingxin Ke, Anton Obukhov, Shengyu Huang, Nando Metzger, Rodrigo Caye Daudt, and Konrad Schindler. 2024. Repurposing Diffusion-Based Image Generators for Monocular Depth Estimation. In *IEEE Conf. Comput. Vis. Pattern Recog.*
- Diederik P. Kingma, Max Welling, et al. 2013. Auto-encoding variational bayes.
- Peter Kocsis, Vincent Sitzmann, and Matthias Nießner. 2024. Intrinsic Image Diffusion for Indoor Single-view Material Estimation. In *IEEE Conf. Comput. Vis. Pattern Recog.*
- Zhengfei Kuang, Yunzhi Zhang, Hong-Xing Yu, Samir Agarwala, Elliott Wu, Jiajun Wu, et al. 2023. Stanford-ORB: a real-world 3D object inverse rendering benchmark. *Advances in Neural Information Processing Systems Datasets and Benchmarks Track*.
- Zhengqin Li, Mohammad Shafiei, Ravi Ramamoorthi, Kalyan Sunkavalli, and Manmohan Chandraker. 2020. Inverse rendering for complex indoor scenes: Shape, spatially-varying lighting and svbrdf from a single image. In *Proceedings of the IEEE/CVF Conference on Computer Vision and Pattern Recognition*. 2475–2484.
- Zhengqi Li and Noah Snavely. 2018. MegaDepth: Learning Single-View Depth Prediction from Internet Photos. In *Computer Vision and Pattern Recognition (CVPR)*.
- Zhibing Li, Tong Wu, Jing Tan, Mengchen Zhang, Jiaqi Wang, and Dahua Lin. 2024. IDArb: Intrinsic Decomposition for Arbitrary Number of Input Views and Illuminations. In *Int. Conf. Learn. Represent.*
- Ruofan Liang, Zan Gojcic, Huan Ling, Jacob Munkberg, Jon Hasselgren, Zhi-Hao Lin, Jun Gao, Alexander Keller, Nandita Vijaykumar, Sanja Fidler, and Zian Wang. 2025. DiffusionRenderer: Neural Inverse and Forward Rendering with Video Diffusion Models. *arXiv preprint arXiv: 2501.18590* (2025).
- Xingchao Liu, Chengyue Gong, and Qiang Liu. 2022. Flow straight and fast: Learning to generate and transfer data with rectified flow. In *Int. Conf. Learn. Represent.*
- Xingchao Liu, Xiwen Zhang, Jianzhu Ma, Jian Peng, and qiang liu. 2024. InstaFlow: One Step is Enough for High-Quality Diffusion-Based Text-to-Image Generation. In *The Twelfth International Conference on Learning Representations*.
- Ilya Loshchilov and Frank Hutter. 2019. Decoupled weight decay regularization. In *Int. Conf. Learn. Represent.*
- Jundan Luo, Duygu Ceylan, Jae Shin Yoon, Nanxuan Zhao, Julien Philip, Anna Frühstück, Wenbin Li, Christian Richardt, and Tuanfeng Wang. 2024. IntrinsicDiffusion: Joint Intrinsic Layers from Latent Diffusion Models. In *ACM SIGGRAPH 2024 Conference Papers*.
- Gonzalo Martin Garcia, Karim Abou Zeid, Christian Schmidt, Daan de Geus, Alexander Hermans, and Bastian Leibe. 2025. Fine-Tuning Image-Conditional Diffusion Models is Easier than You Think. In *Proceedings of the IEEE/CVF Winter Conference on Applications of Computer Vision (WACV)*.
- Chenlin Meng, Robin Rombach, Ruiqi Gao, Diederik P. Kingma, Stefano Ermon, Jonathan Ho, and Tim Salimans. 2022. On Distillation of Guided Diffusion Models. In *IEEE Conf. Comput. Vis. Pattern Recog.*
- Jacob Munkberg, Jon Hasselgren, Tianchang Shen, Jun Gao, Wenzheng Chen, Alex Evans, Thomas Müller, and Sanja Fidler. 2022. Extracting triangular 3d models, materials, and lighting from images. In *IEEE Conf. Comput. Vis. Pattern Recog.* 8280–8290.
- Julien Philip, Sébastien Morgenthaler, Michaël Gharbi, and George Drettakis. 2021. Free-viewpoint Indoor Neural Relighting from Multi-view Stereo. *ACM Trans. Graph.* (2021).
- Robin Rombach, Andreas Blattmann, Dominik Lorenz, Patrick Esser, and Björn Ommer. 2022. High-resolution image synthesis with latent diffusion models. In *IEEE Conf. Comput. Vis. Pattern Recog.* 10684–10695.
- Tim Salimans and Jonathan Ho. 2022. Progressive Distillation for Fast Sampling of Diffusion Models. In *International Conference on Learning Representations*.
- Jiaming Song, Chenlin Meng, and Stefano Ermon. 2020. Denoising diffusion implicit models. *arXiv preprint arXiv:2010.02502* (2020).
- Yang Song, Prafulla Dhariwal, Mark Chen, and Ilya Sutskever. 2023. Consistency models. In *Proceedings of the 40th International Conference on Machine Learning (Honolulu, Hawaii, USA) (ICML '23)*. Article 1335, 42 pages.
- Dor Verbin, Peter Hedman, Ben Mildenhall, Todd Zickler, Jonathan T Barron, and Pratul P Srinivasan. 2022. Ref-nerf: Structured view-dependent appearance for neural radiance fields. In *IEEE Conf. Comput. Vis. Pattern Recog.* 5481–5490.
- Zhou Wang, A.C. Bovik, H.R. Sheikh, and E.P. Simoncelli. 2004. Image quality assessment: from error visibility to structural similarity. *IEEE Transactions on Image Processing* 13, 4 (2004), 600–612. <https://doi.org/10.1109/TIP.2003.819861>
- Zian Wang, Jonah Philion, Sanja Fidler, and Jan Kautz. 2021. Learning Indoor Inverse Rendering with 3D Spatially-Varying Lighting. In *Proceedings of International Conference on Computer Vision (ICCV)*.
- Chen Xi, Peng Sida, Yang Dongchen, Liu Yuan, Pan Bowen, Lv Chengfei, and Zhou. Xiaowei. 2024. IntrinsicAnything: Learning Diffusion Priors for Inverse Rendering Under Unknown Illumination. In *Eur. Conf. Comput. Vis.*
- Guangkai Xu, Yongtao Ge, Mingyu Liu, Chengxiang Fan, Kangyang Xie, Zhiyue Zhao, Hao Chen, and Chunhua Shen. 2024. What Matters When Repurposing Diffusion Models for General Dense Perception Tasks? *arXiv preprint arXiv:2403.06090* (2024).
- Jiamin Xu, Yuxin Zheng, Zelong Li, Chi Wang, Renshu Gu, Weiwei Xu, and Gang Xu. 2025. Detail-Preserving Latent Diffusion for Stable Shadow Removal. In *IEEE Conf. Comput. Vis. Pattern Recog.*
- Chongjie Ye, Lingteng Qiu, Xiaodong Gu, Qi Zuo, Yushuang Wu, Zilong Dong, Liefeng Bo, Yuliang Xiu, and Xiaoguang Han. 2024. StableNormal: Reducing Diffusion Variance for Stable and Sharp Normal. *ACM Trans. Graph.* (2024).
- Tianwei Yin, Michaël Gharbi, Richard Zhang, Eli Shechtman, Frédo Durand, William T Freeman, and Taesung Park. 2024. What Matters When Repurposing Diffusion Distillation. In *IEEE Conf. Comput. Vis. Pattern Recog.*
- Chong Zeng, Yue Dong, Pieter Peers, Youkang Kong, Hongzhi Wu, and Xin Tong. 2024b. DiLightNet: Fine-grained Lighting Control for Diffusion-based Image Generation. In *ACM SIGGRAPH*.
- Zheng Zeng, Valentin Deschaintre, Iliyan Georgiev, Yannick Hold-Geoffroy, Yiwei Hu, Fujun Luan, Ling-Qi Yan, and Miloš Hašan. 2024a. RGBX: Image decomposition and synthesis using material- and lighting-aware diffusion models. In *ACM SIGGRAPH*. <https://doi.org/10.1145/3641519.3657445>
- Shangzhan Zhang, Sida Peng, Tao Xu, Yuanbo Yang, Tianrun Chen, Nan Xue, Yujun Shen, Hujun Bao, Ruizhen Hu, and Xiaowei Zhou. 2024. MaPa: Text-driven Photorealistic Material Painting for 3D Shapes. In *ACM SIGGRAPH 2024 Conference Papers (Denver, CO, USA) (SIGGRAPH '24)*. Association for Computing Machinery, New York, NY, USA, Article 4, 12 pages. <https://doi.org/10.1145/3641519.3657504>
- Yulun Zhang, Yapeng Tian, Yu Kong, Bineng Zhong, and Yun Fu. 2018. Residual dense network for image super-resolution. In *IEEE Conf. Comput. Vis. Pattern Recog.* 2472–2481.
- Jingsen Zhu, Fujun Luan, Yuchi Huo, Zihao Lin, Zhihua Zhong, Dianbing Xi, Rui Wang, Hujun Bao, Jiaxiang Zheng, and Rui Tang. 2022. Learning-Based Inverse Rendering of Complex Indoor Scenes with Differentiable Monte Carlo Raytracing. In *SIGGRAPH Asia 2022 Conference Papers*. ACM, Article 6, 8 pages.
- Zixin Zhu, Xuelu Feng, Dongdong Chen, Jianmin Bao, Le Wang, Yinpeng Chen, Lu Yuan, and Gang Hua. 2023. Designing a better asymmetric vqgan for stablediffusion. *arXiv preprint arXiv:2306.04632* (2023).
- Qi Zuo, Xiaodong Gu, Yuan Dong, Zhengyi Zhao, Weihao Yuan, Lingteng Qiu, Liefeng Bo, and Zilong Dong. 2024. High-Fidelity 3D Textured Shapes Generation by Sparse Encoding and Adversarial Decoding. In *European Conference on Computer Vision*.